





Article

Synthesis, Structure and Magnetic Properties of Low-Dimensional Copper(II) *trans*-1,4-cyclohexanedicarboxylate

Pavel A. Demakov ^{1,*}, Anna A. Ovchinnikova ^{1,2}, Pavel V. Dorovatovskii ³, Vladimir A. Lazarenko ³, Alexander N. Lavrov ¹, Danil N. Dybtsev ¹ and Vladimir P. Fedin ^{1,*}

¹ Nikolaev Institute of Inorganic Chemistry, Siberian Branch of the Russian Academy of Sciences, 630090 Novosibirsk, Russia; a.ovchinnikova5@g.nsu.ru (A.A.O.); lavrov@niic.nsc.ru (A.N.L.); dan@niic.nsc.ru (D.N.D.)

² Department of Natural Sciences, Novosibirsk State University, 630090 Novosibirsk, Russia

³ National Research Centre "Kurchatov Institute", 123182 Moscow, Russia; paulgemi@mail.ru (P.V.D.); vladimir.a.lazarenko@gmail.com (V.A.L.)

* Correspondence: demakov@niic.nsc.ru (P.A.D.); cluster@niic.nsc.ru (V.P.F.)

Abstract: A reaction between copper(II) nitrate and *trans*-1,4-cyclohexanedicarboxylic acid (H₂chdc) carried out under hydrothermal conditions led to a new metal-organic coordination polymer [Cu₂(Hchdc)₂(chdc)]_n. According to single-crystal XRD data, the compound is based on bi-nuclear paddlewheel-type carboxylate blocks that are joined with polymeric chains due to the (μ₃-κ¹:κ²) coordination of carboxylate groups. The chains are interconnected by chdc²⁻ bridging ligands into layers containing free COOH groups of terminal Hchdc⁻. The neighboring layers adopt a RCOOH...OOCR hydrogen bond-assisted arrangement into a dense-packed structure. Magnetization measurements showed the presence of a strong antiferromagnetic exchange interaction (J/k_B = -495 K) inside the bi-nuclear blocks. At the same time, no significant interaction was found between the {-Cu₂(OOCR)₄-} units in spite of their polymeric in-chain packing. Patterns of magnetic behavior of [Cu₂(Hchdc)₂(chdc)]_n were thoroughly analyzed and explained from a structural point of view.

Keywords: coordination polymer; copper(II) complex; carboxylate; X-ray diffraction; magnetization; antiferromagnetism



Citation: Demakov, P.A.; Ovchinnikova, A.A.; Dorovatovskii, P.V.; Lazarenko, V.A.; Lavrov, A.N.; Dybtsev, D.N.; Fedin, V.P. Synthesis, Structure and Magnetic Properties of Low-Dimensional Copper(II) *trans*-1,4-cyclohexanedicarboxylate. *Crystals* **2024**, *14*, 555. <https://doi.org/10.3390/cryst14060555>

Academic Editor: Catherine P. Raptopoulou

Received: 23 May 2024

Revised: 11 June 2024

Accepted: 13 June 2024

Published: 15 June 2024



Copyright: © 2024 by the authors. Licensee MDPI, Basel, Switzerland. This article is an open access article distributed under the terms and conditions of the Creative Commons Attribution (CC BY) license (<https://creativecommons.org/licenses/by/4.0/>).

1. Introduction

Metal-organic coordination polymers (MOCPs) have attracted significant research attention due to their broad structural design [1–3] and targeted modulation of properties that is possible by varying functional metal centers [4], organic ligands [5], and guest substrates [6]. Polynuclear and polymeric blocks consisting of unpaired electron-rich metal ions can present valuable magnetic properties (such as ferro- [7], antiferro- [8], and ferrimagnets [9], as well as slow magnetic relaxation [10,11]), complex luminescence patterns [12,13], redox behavior [14], and unique chemical bonding features [15]. In particular, such metal centers are of interest for the synthesis of MOCPs with designable and unique properties and unveil the usage of coordination polymers in diverse magnetic materials [16], in highly efficient luminophores and sensors [4,17], for data storage [18], and for production of multifunctional and “smart” materials [19].

Copper(II) is one of the readily available ions with valuable functional characteristics, and it is widely used in MOCP chemistry [20,21]. The redox activity and optical properties of Cu²⁺ are applicable in the design of catalysts and photocatalysts [22,23], while the relative structural rigidity of its coordination environment increases the predictability of the polymer lattice [24]. The paramagnetism of Cu²⁺ ion ($S = 1/2$) can provide deep insights into the structural dynamics and the nature of adsorption centers in mechanistic studies [25–27], by means of physical methods, and allows us to achieve an extremely strong magnetic exchange in its polymeric complexes [28,29]. In this work, a new MOCP

with the formula $[\text{Cu}_2(\text{Hchdc})_2(\text{chdc})]_n$ (**I**), containing differently charged anions of *trans*-1,4-cyclohexanedicarboxylic acid (H_2chdc), being also readily available but mildly spread in coordination chemistry [30], as ligands, was structurally characterized. A $(\mu_3\text{-}\kappa^1\text{:}\kappa^2)$ coordination of the carboxylates and hydrogen bonds between them and free carboxylic groups induce a formation of a corrugated layered structure based on 1D chains of magnetoactive Cu^{2+} ions. However, magnetic measurements demonstrated that these copper-carboxylate chains represent a set of weakly interacting antiferromagnetic dimers with a very strong ($J/k_B = -495$ K) inner exchange and a pronounced influence of structural defects regarding their low-temperature magnetization behavior.

2. Materials and Methods

2.1. Materials

Copper(II) nitrate trihydrate (analytical reagent; Chimmed, Moscow, Russian Federation), *trans*-1,4-cyclohexanedicarboxylic acid (H_2chdc , >97.0%; TCI, Tokyo, Japan), and acetone (reagent grade; Vekton, Saint Petersburg, Russian Federation) were used as received. Distilled water was used in all synthetic experiments.

2.2. Instruments

Bruker Scimitar FTS 2000 spectrometer (Billerica, MA, USA) was used to obtain infrared (IR) spectra in the range of 4000–400 cm^{-1} with KBr pellets. VarioMICROcube analyzer (Elementar Analysensysteme GmbH, Hanau, Germany) was used for elemental CHNS analyses. Bruker D8 Advance diffractometer (Cu-K α radiation, $\lambda = 1.54178$ Å; Billerica, MA, USA) was used for powder X-ray diffraction (PXRD) data acquisition at room temperature. Netzsch TG 209 F1 Iris device (Selb, Germany) was used for thermogravimetric analysis under Ar flow (30 $\text{cm}^3 \cdot \text{min}^{-1}$) at a 10 $\text{K} \cdot \text{min}^{-1}$ heating rate.

A Quantum Design MPMS-XL (San Diego, CA, USA) SQUID magnetometer was used to measure the magnetic susceptibility of $[\text{Cu}_2(\text{Hchdc})_2(\text{chdc})]_n$ (**I**) in the temperature range of 1.77–300 K under applied magnetic fields $H = 0$ –10 kOe. The measured values of the total molar susceptibility, $\chi = M/H$, were corrected for the temperature-independent diamagnetic core contribution, χ_d , calculated using the Pascal's additive scheme, which allowed us to determine the paramagnetic component of the magnetic susceptibility, $\chi_p(T)$. To check for the presence of ferromagnetic trace impurities in the sample, we measured isothermal $M(H)$ dependencies at several temperatures and took $M(T)$ data in various magnetic fields; a weak FM contribution, $\chi_{\text{FM}}(T)$, was indeed detected in this way and subtracted from the data. Due to the low magnetic susceptibility of the sample and its low amount available, 4 cycles of measurements were carried out in the range of 1.77–300 K at both heating and cooling to increase the accuracy of measurements and confirm their reproducibility.

2.3. Synthetic Methods

Synthesis of $[\text{Cu}_2(\text{Hchdc})_2(\text{chdc})]_n$ (**I**). $\text{Cu}(\text{NO}_3)_2 \cdot 3\text{H}_2\text{O}$ (1.67 g, 6.9 mmol), H_2chdc (1.46 g, 8.5 mmol), and 25.0 mL of water were mixed in a Teflon liner (50 mL general volume). The liner was placed into a stainless steel autoclave and heated at 120 °C during 48 h with 50 °C \cdot h $^{-1}$ heating and cooling rates. After cooling, the obtained white-blue crystalline precipitate was washed with water (~20 mL) and then with acetone (~5 mL) and dried in air. Yield: 5%. IR spectrum main bands (KBr, cm^{-1}): 3191 $\nu(\text{O-H}_{\text{COOH}})$, 2944 $\nu(\text{C}(\text{sp}^3)\text{-H}_{\text{CHring}})$, 2853 $\nu(\text{C}(\text{sp}^3)\text{-H}_{\text{CH}_2\text{ring}})$, 1728 $\nu(\text{CO}_{\text{COOH}})$, 1585 $\nu_{\text{as}}(\text{COO}^-)$, and 1416 $\nu_{\text{s}}(\text{COO}^-)$. Elemental CHN analysis, calculated for $[\text{Cu}_2(\text{Hchdc})_2(\text{chdc})]_n$ ($\text{C}_{24}\text{H}_{32}\text{O}_{12}\text{Cu}_2$) (%): C 45.1; H 5.0; N 0.0. Found (%): C 45.0; H 5.0; N 0.0.

2.4. Single Crystal X-ray Diffraction Details

Diffraction data for single crystals of **I** were collected on the 'Belok' beamline [31,32] ($\lambda = 0.74503$ Å) of the National Research Center 'Kurchatov Institute' (Moscow, Russian Federation) using a Rayonix SX165 CCD detector. XDS program (Version 10 January 2022) package [33] was used for data indexing, integration, scaling, and absorption correction.

Dual-space algorithm (SHELXT [34]) was used for structure solution, and the full-matrix least squares technique (SHELXL [35]) was used for structure refinement. Anisotropic approximation was applied for all atoms, except hydrogens. Positions of C-bonded hydrogen atoms were calculated geometrically and refined in the riding model. Positions of O-bonded H atoms were found directly and further refined with the application of DFIX restraints for stable refinement. A non-merohedral twinning with an orientation matrix $(-1\ 0\ 0\ 0\ -1\ 0\ -0.426\ -0.199\ 1)$ and second component weight (BASF) of ca. 0.34 was found and analyzed using PLATON [36] software (Version 13 May 2024) after finding a structural model and its primary refinement. Details for single-crystal structure determination experiments and structure refinements are summarized in Table 1. CCDC 2309813 (I) entry contains the supplementary crystallographic data for this paper. These data can be obtained free of charge from The Cambridge Crystallographic Data Center at <https://www.ccdc.cam.ac.uk/structures/> (accessed on 12 June 2024).

Table 1. Single-crystal X-ray diffraction and structure refinement details.

Parameter	I
Chemical formula	C ₁₂ H ₁₆ CuO ₆
<i>M_r</i> , g·mol ^{−1}	319.79
Crystal system	Triclinic
Space group	<i>P</i> ^{−1}
<i>a</i> , Å	5.160(1)
<i>b</i> , Å	10.820(2)
<i>c</i> , Å	22.630(5)
Temperature, K	100
α, °	86.95(3)
β, °	86.90(3)
γ, °	83.34(3)
<i>V</i> , Å ³	1251.7(4)
<i>Z</i>	4
<i>D_{calc}</i> , g·cm ^{−3}	1.697
μ, mm ^{−1}	1.99
F(000)	660
Crystal size, mm	0.04 × 0.02 × 0.02
θ range for data collection, °	2.0 ≤ θ ≤ 26.55
Index ranges	−6 ≤ <i>h</i> ≤ 6; −13 ≤ <i>k</i> ≤ 13; −3 ≤ <i>l</i> ≤ 27
No. of reflections: measured/independent/observed [<i>I</i> > 2σ(<i>I</i>)]	4376/4376/4145
<i>R_{int}</i>	–
Goodness-of-fit on <i>F</i> ²	1.221
Final <i>R</i> indices [<i>I</i> > 2σ(<i>I</i>)]	<i>R</i> ₁ = 0.1024; <i>wR</i> ₂ = 0.2961
Final <i>R</i> indices [all data]	<i>R</i> ₁ = 0.1045; <i>wR</i> ₂ = 0.2970
Largest diff. peak, hole, e·Å ^{−3}	1.90, −1.75

3. Results and Discussion

3.1. Synthesis

Compound $[\text{Cu}_2(\text{Hchdc})_2(\text{chdc})]_n$ (**I**) was obtained in a single-crystalline phase in low yield by heating a mixture of copper(II) nitrate and H_2chdc in water in a stainless steel autoclave with a Teflon liner at $120\text{ }^\circ\text{C}$ for 48 h. After cooling the reaction mixture to room temperature, the solid mixture contained blue single crystals of **I** and colorless crystals of unreacted *trans*-1,4-cyclohexanedicarboxylic acid. Then, H_2chdc was removed by washing the precipitate with acetone to obtain **I** in a pure form. Attempts to increase the target product yield by adding potassium hydroxide or several weak organic bases (such as 1,4-diazabicyclo[2.2.2]octane, urotropine, triethylamine, urea, *N,N*-dimethylformamide) to the reaction mixture, as well as by increasing the temperature of the synthesis, led to the admixtures of the previously reported $[\text{Cu}_2(\text{chdc})_2]$ [37] or unidentified copper-containing products.

3.2. Crystal Structure

According to SCXRD results, **I** crystallized in the triclinic system with the $P\bar{1}$ space group. **I** contains two independent Cu(II) ions. Both Cu(1) and Cu(2) have a similar square/pyramidal coordination polyhedron, consisting of five oxygen atoms from five COO groups, two of which have a $(\mu_2-\kappa^1:\kappa^1)$ coordination, and three more adopt the $(\mu_3-\kappa^1:\kappa^2)$ coordination (Figure 1a). Cu–O bond lengths are very close for both independent metal ions and lie in the range of 1.947(7)–1.996(7) Å for O atoms of pyramid bases and are 2.204(6) Å, 2.210(6) Å for the pyramid vertices. Such coordination modes of carboxylate groups lead to the formation of paddlewheel blocks condensed through the O atoms of μ_3 -COO groups into polymeric $\{-\text{Cu}_2(\text{OOCR})_4-\}_n$ chains lying along *a* crystallographic axis. The Cu...Cu distances inside paddlewheels are 2.571(2) Å and 2.576(2) Å, and the shortest interblock Cu...Cu distances are 3.21–3.22 Å, which can suggest strong exchange interactions between paramagnetic metal ions both inside the bi-nuclear blocks and between them—along polymeric chains. Nearby chains are interlinked along the *b* axis by bridging *trans*-1,4-cyclohexanedicarboxylates (chdc^{2-}) into layers (Figure 1b). Monoprotonated Hchdc^- ligands containing uncoordinated COOH groups are coordinated to the chains almost perpendicularly to the *ab* planes (Figure 1c), forming interlayer $\text{H}(\text{COOH})\cdots\text{O}(\text{COO})$ hydrogen bonds with the corresponding oxygen–oxygen distances of 2.72–2.73 Å. The resulting three-dimensional packing of layers in **I** does not contain any significant voids.

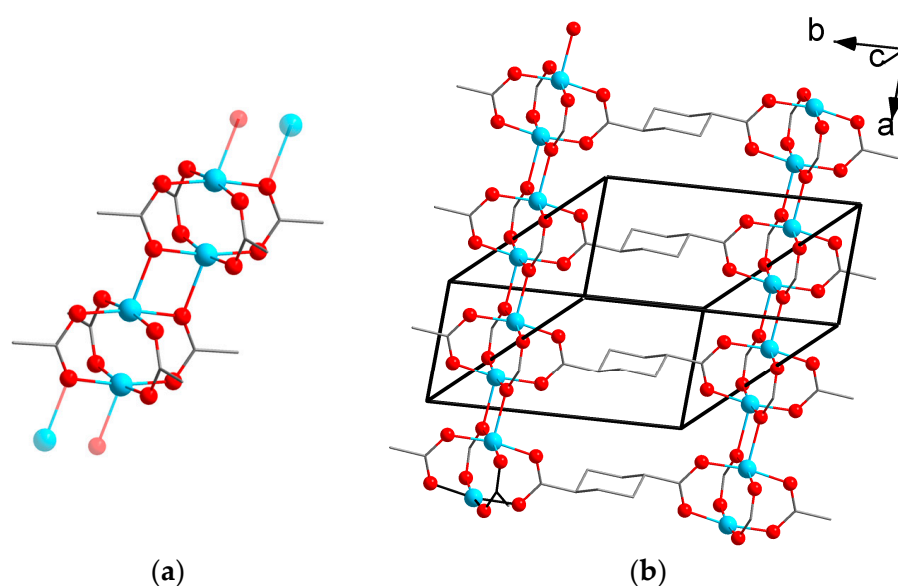


Figure 1. Cont.

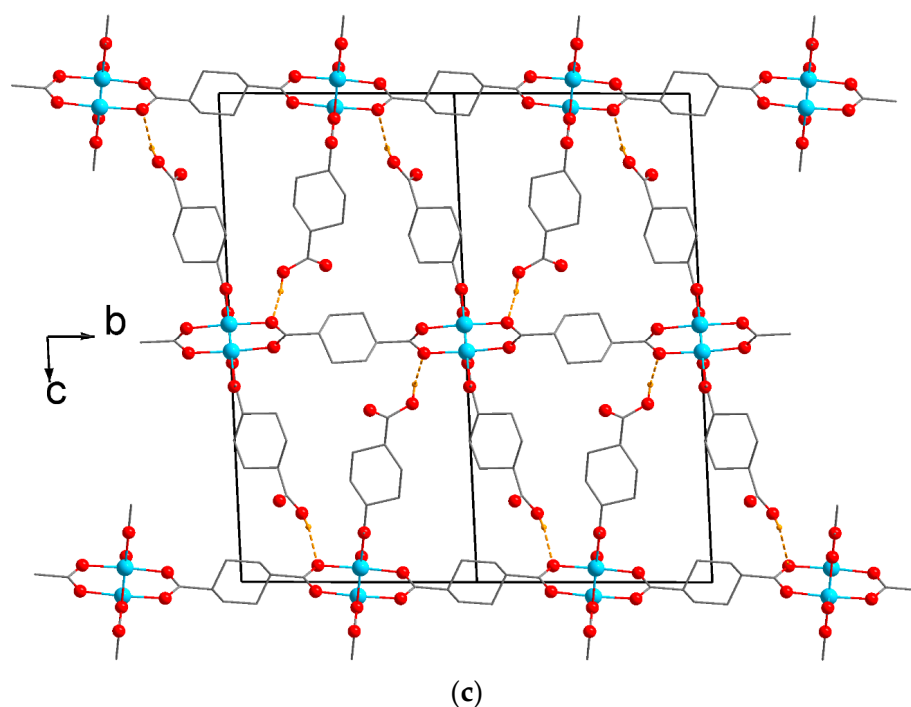


Figure 1. $\{Cu_2(OOCR)_4\}$ bi-nuclear blocks and their connection in the structure of **I** (a). Coordination network in **I**; view along c axis (b). Three-dimensional package of **I**; view along a axis (c). Copper atoms are shown in blue; oxygen atoms are shown in red. Hydrogen bonds are shown by orange dashed lines.

3.3. Phase Purity and Characterization

The phase purity of **I** was confirmed by powder X-ray diffraction (PXRD, Figure 2a). Elemental (CHN) analysis results are in full agreement with the chemical formula $[Cu_2(Hchdc)_2(chdc)]_n$ obtained from the SCXRD data. The IR spectrum of **I** contains characteristic absorption bands of $C(sp^3)-H$ stretching vibrations at 2944 cm^{-1} and 2853 cm^{-1} , $C=O$ stretching vibrations in the free COOH group at 1728 cm^{-1} , symmetric and antisymmetric vibrations of the coordinated carboxyl group at 1416 cm^{-1} and 1585 cm^{-1} , respectively, and a broad absorption band of O–H stretching vibrations at $\sim 3200\text{ cm}^{-1}$. According to thermogravimetric analysis (TGA) data, the sample is stable up to $300\text{ }^\circ\text{C}$. The first step of weight loss is observed at $345\text{ }^\circ\text{C}$ (Figure 2b). The residual weight after the first decomposition step is 48%, corresponding well to the presumable formula $Cu_2O(chdc)$ for the intermediate decomposition product (49.0% theoretical weight). The second weight loss step is observed at $390\text{ }^\circ\text{C}$. The final weight residue after the second stage is 22% and corresponds well to Cu_2O as the final product for the decomposition of **I** (22.4% theoretical weight) in an inert atmosphere. Such a stepwise shape of the TGA curve is similar to the examples within the literature for other “acidic” *trans*-1,4-cyclohexanedicarboxylates, such as non-isostructural $[Mn_2(Hchdc)_2(chdc)]_n$ [38].

3.4. Magnetization Data

The magnetic susceptibility $\chi = M/H$ of complex **I**, measured during thermal cycling of the sample in the temperature range of 1.77–300 K, did not depend on either its thermomagnetic history or the magnetic field strength, except for at lower temperatures, where the field dependence $\chi(H)$ fitted well to the Brillouin function for paramagnetic ions with spin $S = 1/2$. The paramagnetic component of the magnetic susceptibility χ_p (Figure 3a), obtained after subtracting the temperature-independent diamagnetic contribution, was $\approx 1.5 \cdot 10^{-3}\text{ emu/mol}$ at 300 K and gradually decreased almost to zero upon cooling the sample from room temperature to 50–60 K. Such a pronounced drop in magnetic susceptibility indicates not only the presence of strong antiferromagnetic (AF) interactions between Cu^{2+} ions but also the formation of a gap in the spectrum of spin excitations in the system;

without such a gap, significant magnetic susceptibility would persist, even in a completely ordered AF state. The occurrence of a spin gap along with the smooth decrease in χ_p are known to be the typical manifestations of AF-coupled dimers [39] and dimer-derived structures. This observation appears in perfect agreement with the crystal structure of complex I based on polymeric chains of bi-nuclear Cu(II)-carboxylate blocks (Figure 1). The strength of the AF interaction can be seen clearly in the $\chi_p T(T)$ graph (Figure 3b), where $\chi_p T$ is almost zero at temperatures below 60–70 K and reaches only half the value that would be observed for the two Cu²⁺ ions in $[\text{Cu}_2(\text{Hchdc})_2(\text{chdc})]_n$ at room temperature—in the absence of an interaction between them.

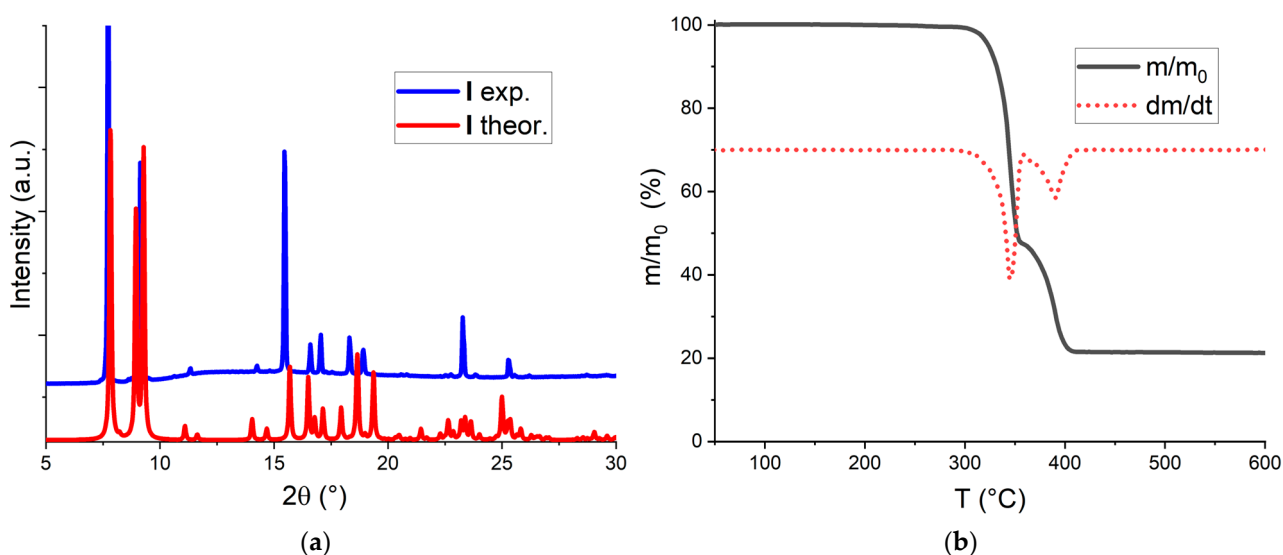


Figure 2. Powder X-ray diffraction pattern of sample I compared to the theoretical one (a). TGA curve and dm/dT plot for I (b).

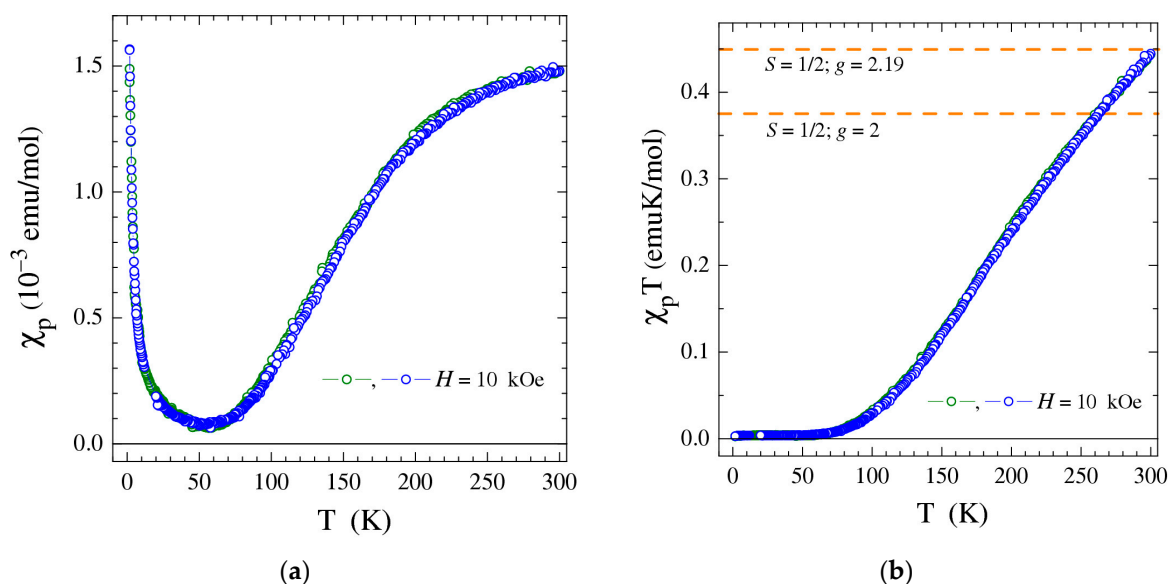


Figure 3. Temperature dependences of χ_p (a) and $\chi_p T$ (b) of complex I measured in a magnetic field $H = 10$ kOe. Each curve was obtained by averaging two series of measurements. The dashed lines in graph (b) show the levels corresponding to one ion with spin $S = 1/2$ and g -factors $g = 2.0$; 2.19 .

In the low-temperature region ($T < 60$ K), an increase in χ_p is observed (Figure 3a), which is associated with the presence of impurities retaining their paramagnetic state down to the minimal temperature $T = 1.77$ K. An impurity paramagnetism of sample I

apparently arises from the decomposition of bi-nuclear blocks in near-surface crystallite defects with the formation of single Cu^{2+} ions [40]. As can be seen from Figure 3a, there is virtually no overlap of temperature ranges at points where significant contributions to the magnetic susceptibility of AF dimers ($T \geq 70$ K) and paramagnetic impurities ($T \leq 50$ K) are observed. This allows the concentration and magnetic parameters of single Cu^{2+} ions to be determined by simply approximating the low-temperature $\chi_p(T)$ data (Figure 4) using the Curie–Weiss dependence $\chi_{\text{CW}}(T) = N_A \mu_{\text{eff}}^2 / 3k_B(T - \theta)$ —where N_A and k_B are the Avogadro number and the Boltzmann constant, respectively, μ_{eff} is the effective magnetic moment of a single Cu^{2+} ion, and θ is the Weiss constant—reflecting its interaction with neighboring copper ions. In turn, the analysis of the $\chi_p(T)$ dependence in the region $T \geq 70$ K has shown good agreement with the behavior theoretically predicted for AF Cu^{2+} – Cu^{2+} dimers [39]. Accordingly, a quantitative analysis of the data over the entire temperature range was carried out using the modified Bleaney–Bowers formula [39], which takes into account the presence of AF dimers and monomer molecules:

$$\chi_p(T) = (1 - \delta)\chi_{\text{dim}} + 2\delta\chi_{\text{CW}} = (1 - \delta)(2N_A \mu_B^2 g^2 / 3k_B T) / [1 + \exp(-J/k_B T) / 3] + 2\delta\chi_{\text{CW}}, \quad (1)$$

where χ_{dim} and χ_{CW} are the magnetic susceptibilities of dimers and monomers, respectively; δ is the mole fraction of dimers transformed into monomers; g is the g-factor of Cu^{2+} ions (assumed to be the same for dimers and monomers); and J is the exchange interaction energy between copper ions in dimers described by the Hamiltonian $H = -J \vec{S}_1 \cdot \vec{S}_2$. As can be seen in Figure 5, the experimental data can be approximated very well using Formula (1) with parameters $J/k_B \approx -495$ K; $g \approx 2.19$; $\delta \approx 0.45$ mol. %.

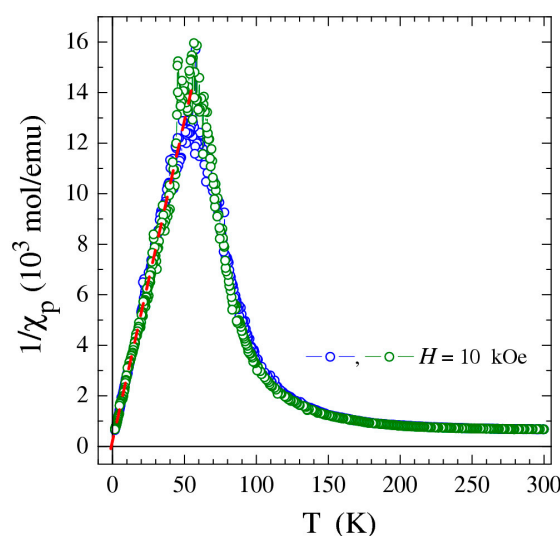


Figure 4. Temperature dependences of $1/\chi_p$ of complex **I** measured in a magnetic field $H = 10$ kOe. The dashed line shows the approximation of low-temperature data using the Curie–Weiss dependence.

Since the dimer blocks are assembled into polymer chains within the crystal structure of complex **I**, a more rigorous analysis of the magnetic properties should be carried out using the model of partially dimerized chains described by the Hamiltonian $H = -J \sum_i^{n/2} (\vec{S}_{2i-1} \cdot \vec{S}_{2i} + \alpha \vec{S}_{2i} \cdot \vec{S}_{2i+1})$, where the inter-dimer interaction $J' = \alpha J$ is also considered in addition to the intra-dimer Cu^{2+} – Cu^{2+} exchange J [41]. However, upon applying this model, no further improvement exceeding the experimental error was obtained in the description of the $\chi_p(T)$ data, which indicates that the interaction between the blocks is very weak ($J' \ll J$).

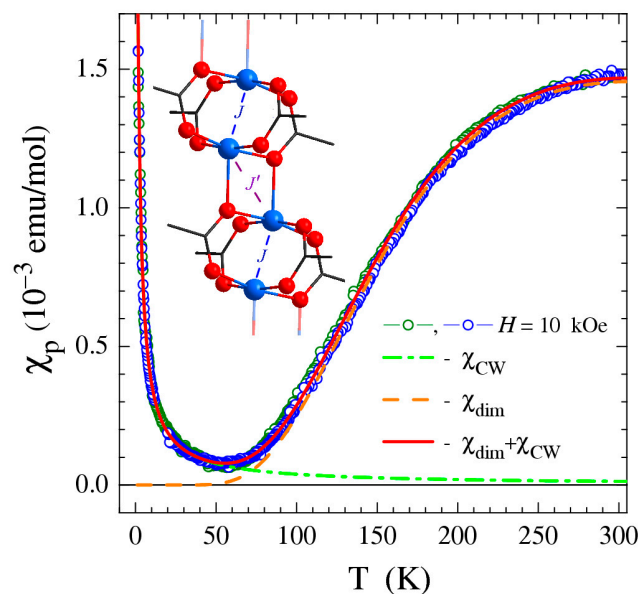


Figure 5. Experimental $\chi_p(T)$ data for complex I (symbols) and their approximation by the theoretical expression obtained using the Bleaney–Bowers model (solid line). Contributions from dimers and monomers are shown by the dashed and dash-dotted lines, respectively. The inset illustrates the chain built from AF dimers with strong intra-dimer coupling J , and a weak interaction between dimers J' .

Despite the apparent consistency between magnetization and structural data, one may wonder whether the identification of bi-nuclear paddlewheel fragments of polymer chains as AF Cu^{2+} - Cu^{2+} dimers, weakly coupled with each other magnetically, is actually correct. Indeed, at a first glance, the exchange-interaction pathways through Cu-O-Cu bonds (inset to Figure 5) may seem preferable over the Cu-O-C-O-Cu ones. However, this is not the case; both the strong AF coupling in the paddlewheel blocks and the weak superexchange interaction through Cu-O-Cu bonds of the geometry in complex I are confirmed by many sources of data within the literature on similar compounds. The most clear example is the compound $[\text{Cu}_2\text{Y}_2\text{L}_{10}(\text{H}_2\text{O})_4 \cdot 3\text{H}_2\text{O}]_n$, where HL = *trans*-2-butenoic (crotonic) acid, in which $\{\text{Cu}_2(\text{OOCR})_4\}$ paddlewheel units in polymer chains are spatially separated by diamagnetic bi-nuclear $\{\text{Y}_2(\text{OOCR})_6\}$ blocks and are thus magnetically isolated from each other [42]. The value of the AF exchange interaction in isolated copper(II)-based paddlewheel dimer units was found to be $J/k_B \approx -486$ K [41], appearing very close to the value -495 K obtained in this work. Even closer magnetic parameters ($J/k_B \approx -493$ K; $g \approx 2.188$) were defined for isolated $\{\text{Cu}_2(\text{OOCR})_4\}$ blocks in ref. [37]. In turn, studies of di-nuclear Cu(II) complexes with Cu_2O_2 cores possessing a geometry similar to complex I have revealed only a weak ($|J/k_B| \sim 5$ K) exchange interaction through Cu-O-Cu bonds, whose sign is dependent on the Cu-O-Cu angle [43].

Among the compounds based on $\{-\text{Cu}_2(\text{OOCR})_4-\}_n$ polymeric chains [28,37,44], the closest ones to complex I parameters ($J/k_B = -485$ K; $g = 2.207$) were reported for layered compound $[\text{Cu}_2(\text{cis,cis-1,3,5-Hctc})_2]_n$ [37], where 1,3,5- H_3ctc = 1,3,5-cyclohexanetricarboxylic acid. For all the referenced chain-based compounds, the insignificance of the exchange interaction between bi-nuclear blocks was emphasized [28,37,44], and only the authors in ref. [28] qualitatively determined the value of $J'/k_B \approx 8.5$ K, which appears to be almost two orders of magnitude smaller than the interaction within the dimer units (J/k_B). It should be noted that in all the listed works, impurity paramagnetism (described by the Curie–Weiss model) was observed at $T < 50$ K, and it was typically subtracted empirically and not analyzed in detail. We can suggest that such a feature of complex I is associated with the destruction of paddlewheel units in the near-surface defects of crystallites, forming monomer paramagnetic ions. According to the parameter $\delta \approx 0.45$ mol. % (reflecting the fraction of decomposed dimers as $\approx 1/220$), the average number of paddlewheel blocks in a single $\{-\text{Cu}_2(\text{OOCR})_4-\}_n$ chain should be $n \approx 220$. Using the cell parameter $a = 5.16$ Å, whose

crystallographic vector is aligned parallel to the chains, the average length of defect-free copper(II)-carboxylate chains in complex I can be estimated as $(220 \cdot 0.516 \approx 114)$ nm, which is quite large and consistent with high crystallinity shown by PXRD results.

4. Conclusions

To summarize, a new metal-organic coordination polymer of copper(II), which contains differently charged *trans*-1,4-cyclohexanedicarboxylate anions, was synthesized. The compound is based on two-dimensional coordination layers, while its magnetically active substructure is represented by one-dimensional copper-carboxylate chains. The packing of layers within the crystal structure is supported by hydrogen bonds between protonated (uncoordinated) carboxyl groups and bound carboxylate anions. Magnetization measurements have shown the presence of strong antiferromagnetic interactions ($J/k_B = -495$ K) in $\{Cu_2(OOCR)_4\}$ paddlewheel units without any significant exchange between even the closest bi-nuclear fragments.

Author Contributions: Conceptualization, P.A.D. and V.P.F.; methodology, P.A.D., A.N.L. and D.N.D.; software, A.N.L., P.V.D. and V.A.L.; validation, P.A.D. and V.P.F.; formal analysis, A.N.L.; investigation, A.A.O. (synthesis, characterization, graphing), A.N.L. (magnetization measurements, graphing), P.V.D. (single-crystal XRD), V.A.L. (single-crystal XRD); resources, D.N.D. and V.P.F.; data curation, P.V.D., V.A.L. and V.P.F.; writing—original draft preparation, P.A.D., A.A.O. and A.N.L.; writing—review and editing, D.N.D. and V.P.F.; visualization, P.A.D., A.A.O. and A.N.L.; supervision, P.A.D.; project administration, V.P.F.; funding acquisition, V.P.F. All authors have read and agreed to the published version of the manuscript.

Funding: The authors are grateful to the Ministry of Science and Higher Education of the Russian Federation for financial support (Agreement No. 075-15-2022-263), and for providing access to the large-scale research facility “EXAFS spectroscopy beamline”.

Data Availability Statement: CCDC 2309813 entry contains the supplementary crystallographic data for this paper. This original data presented in the study are openly available in The Cambridge Crystallographic Data Center at <https://www.ccdc.cam.ac.uk/structures/> (accessed on 12 June 2024). Other characterization method original datasets will be made available on request from the corresponding authors due to privacy.

Conflicts of Interest: The authors declare no conflicts of interest.

References

1. Yaghi, O.M.; O’Keeffe, M.; Ockwig, N.W.; Chae, H.K.; Eddaoudi, M.; Kim, J. Reticular synthesis and the design of new materials. *Nature* **2003**, *423*, 705–714. [[CrossRef](#)]
2. Barsukova, M.; Sapijanik, A.; Guillermin, V.; Shkurenko, A.; Shaikh, A.C.; Parvatkar, P.; Bhatt, P.M.; Bonneau, M.; Alhaji, A.; Shekhah, O.; et al. Face-directed assembly of tailored isoreticular MOFs using centring structure-directing agents. *Nat. Synth.* **2024**, *3*, 33–46. [[CrossRef](#)]
3. Zhang, Q.; Yan, S.; Yan, X.; Lv, Y. Recent advances in metal-organic frameworks: Synthesis, application and toxicity. *Sci. Total Environ.* **2023**, *902*, 165944. [[CrossRef](#)]
4. Lunev, A.M.; Belousov, Y.V. Luminescent sensor materials based on rare-earth element complexes for detecting cations, anions, and small molecules. *Russ. Chem. Bull.* **2022**, *71*, 825–857. [[CrossRef](#)]
5. Zaguzin, A.S.; Sukhikh, T.; Sokolov, M.N.; Fedin, V.P.; Adonin, S.A. Zn(II) Three-Dimensional Metal-Organic Frameworks Based on 2,5-Diiodoterephthalate and N,N Linkers: Structures and Features of Sorption Behavior. *Inorganics* **2023**, *11*, 192. [[CrossRef](#)]
6. Sun, Z.; Khurshid, A.; Sohail, M.; Qiu, W.; Cao, D.; Su, S.J. Encapsulation of Dyes in Luminescent Metal-Organic Frameworks for White Light Emitting Diodes. *Nanomaterials* **2021**, *11*, 2761. [[CrossRef](#)]
7. Wu, Y.; Cheng, S.; Liu, J.; Yang, G.; Wang, Y.Y. New porous Co(II)-based metal-organic framework including 1D ferromagnetic chains with highly selective gas adsorption and slow magnetic relaxation. *J. Solid State Chem.* **2019**, *276*, 226–231. [[CrossRef](#)]
8. Gong, T.; Li, P.; Sui, Q.; Zhou, L.J.; Yang, N.N.; Gao, E.Q. Switchable Ferro-, Ferri-, and Antiferromagnetic States in a Piezo- and Hydrochromic Metal–Organic Framework. *Inorg. Chem.* **2018**, *57*, 6791–6794. [[CrossRef](#)] [[PubMed](#)]
9. Mahata, P.; Sen, D.; Natarajan, S. A three-dimensional metal–organic framework with a distorted Kagome related layer showing canted antiferromagnetic behaviour. *Chem. Commun.* **2008**, *2008*, 1278–1280. [[CrossRef](#)]
10. Kuppusamy, S.K.; Moreno-Pineda, E.; Nonat, A.M.; Heinrich, B.; Karmazin, L.; Charbonniere, L.J.; Ruben, M. Binuclear Lanthanide Complexes Based on 4-Picoline-N-oxide: From Sensitized Luminescence to Single-Molecule Magnet Characteristics. *Cryst. Growth Des.* **2023**, *23*, 1084–1094. [[CrossRef](#)]

11. Matyukhina, A.K.; Zorina-Tikhonova, E.N.; Goloveshkin, A.S.; Babeshkin, K.A.; Efimov, N.N.; Kiskin, M.A.; Eremenko, I.L. Field-Induced Slow Magnetic Relaxation in Co^{II} Cyclopropane-1,1-dicarboxylates. *Molecules* **2022**, *27*, 6537. [[CrossRef](#)] [[PubMed](#)]
12. Salaam, J.; Tabti, L.; Bahamyirou, S.; Lecointre, A.; Hernandez Alba, O.; Jeannin, O.; Camerel, F.; Cianfèrani, S.; Bentouhami, E.; Nonat, A.M.; et al. Formation of Mono- and Polynuclear Luminescent Lanthanide Complexes based on the Coordination of Preorganized Phosphonated Pyridines. *Inorg. Chem.* **2018**, *57*, 6095–6106. [[CrossRef](#)] [[PubMed](#)]
13. Ivanova, E.A.; Smirnova, K.S.; Pozdnyakov, I.P.; Potapov, A.S.; Lider, E.V. Photoluminescent Lanthanide(III) Coordination Polymers with Bis(1,2,4-Triazol-1-yl)Methane Linker. *Inorganics* **2023**, *11*, 317. [[CrossRef](#)]
14. Litvinova, Y.M.; Gayfulin, Y.M.; Kovalenko, K.A.; Samsonenko, D.G.; Van Leusen, J.; Korolkov, I.V.; Fedin, V.P.; Mironov, Y.V. Multifunctional Metal–Organic Frameworks Based on Redox-Active Rhenium Octahedral Clusters. *Inorg. Chem.* **2018**, *57*, 2072–2084. [[CrossRef](#)] [[PubMed](#)]
15. Afonin, M.Y.; Konokhova, A.Y.; Dmitriev, A.A.; Abramov, P.A.; Kuratieva, N.V.; Sukhikh, T.S.; Kompankov, N.B.; Gritsan, N.P.; Konchenko, S.N. Chromium–Lanthanide Complexes Containing the Cr=P=Cr Fragment: Synthesis, Characterization, and Computational Study. *Inorg. Chem.* **2023**, *62*, 10110–10119. [[CrossRef](#)] [[PubMed](#)]
16. Mínguez Espallargas, G.; Coronado, E. Magnetic functionalities in MOFs: From the framework to the pore. *Chem. Soc. Rev.* **2018**, *47*, 533–557. [[CrossRef](#)] [[PubMed](#)]
17. Yu, X.; Ryadun, A.A.; Pavlov, D.I.; Guselnikova, T.Y.; Potapov, A.S.; Fedin, V.P. Highly Luminescent Lanthanide Metal–Organic Frameworks with Tunable Color for Nanomolar Detection of Iron(III), Ofloxacin and Gossypol and Anti-counterfeiting Applications. *Angew. Chem. Int. Ed.* **2023**, *135*, e202306680. [[CrossRef](#)]
18. Yang, C.; Dong, R.; Wang, M.; Petkov, P.S.; Zhang, Z.; Wang, M.; Han, P.; Ballabio, M.; Bräuninger, S.A.; Liao, Z.; et al. A semiconducting layered metal-organic framework magnet. *Nat. Commun.* **2019**, *10*, 3260. [[CrossRef](#)] [[PubMed](#)]
19. Zhang, T.; Hu, Y.Q.; Mo, Z.W.; Liao, P.Q.; Sakiyama, H.; Han, T.; Chen, X.M.; Zheng, Y.Z. Cobalt(II) Magnetic Metal–Organic Framework with an Effective Kagomé Lattice, Large Surface Area, and High Spin-Canted Ordering Temperature. *ACS Appl. Mater. Interfaces* **2017**, *9*, 38181–38186. [[CrossRef](#)]
20. Cun, J.E.; Fan, X.; Pan, Q.; Gao, W.; Luo, K.; He, B.; Pu, Y. Copper-based metal–organic frameworks for biomedical applications. *Adv. Colloid Interface Sci.* **2022**, *305*, 102686. [[CrossRef](#)]
21. Stirk, A.J.; Wilson, B.H.; O’Keefe, C.A.; Amarne, H.; Zhu, K.; Schurko, R.W.; Loeb, S.J. Applying reticular synthesis to the design of Cu-based MOFs with mechanically interlocked linkers. *Nano Res.* **2021**, *14*, 417–422. [[CrossRef](#)]
22. An, B.; Li, Z.; Song, Y.; Zhang, J.; Zeng, L.; Wang, C.; Lin, W. Cooperative copper centres in a metal–organic framework for selective conversion of CO₂ to ethanol. *Nat. Catal.* **2019**, *2*, 709–717. [[CrossRef](#)]
23. Nwosu, U.; Siahrostami, S. Copper-based metal–organic frameworks for CO₂ reduction: Selectivity trends, design paradigms, and perspectives. *Catal. Sci. Technol.* **2023**, *13*, 3740–3761. [[CrossRef](#)]
24. Liu, J.; Lukose, B.; Shekhah, O.; Arslan, H.K.; Weidler, P.; Gliemann, H.; Bräse, S.; Grosjean, S.; Godt, A.; Feng, X.; et al. A novel series of isorecticular metal organic frameworks: Realizing metastable structures by liquid phase epitaxy. *Sci. Rep.* **2012**, *2*, 921. [[CrossRef](#)] [[PubMed](#)]
25. Demakov, P.A.; Poryvaev, A.S.; Kovalenko, K.A.; Samsonenko, D.G.; Fedin, M.V.; Fedin, V.P.; Dybtsev, D.N. Structural Dynamics and Adsorption Properties of the Breathing Microporous Aliphatic Metal–Organic Framework. *Inorg. Chem.* **2020**, *59*, 15724–15732. [[CrossRef](#)] [[PubMed](#)]
26. Mendt, M.; Ehrling, S.; Senkovska, I.; Kaskel, S.; Pöppl, A. Synthesis and Characterization of Cu–Ni Mixed Metal Paddlewheels Occurring in the Metal–Organic Framework DUT-8(Ni_{0.98}Cu_{0.02}) for Monitoring Open-Closed-Pore Phase Transitions by X-Band Continuous Wave Electron Paramagnetic Resonance Spectroscopy. *Inorg. Chem.* **2019**, *58*, 4561–4573. [[CrossRef](#)] [[PubMed](#)]
27. Kolganov, A.A.; Gabrienko, A.A.; Stepanov, A.G. Reaction of methane with benzene and CO on Cu-modified ZSM-5 zeolite investigated by ¹³C MAS NMR spectroscopy. *Chem. Phys. Lett.* **2023**, *810*, 140188. [[CrossRef](#)]
28. Perec, M.; Baggio, R.; Sartoris, R.P.; Santana, R.C.; Peña, O.; Calvo, R. Magnetism and Structure in Chains of Copper Dinuclear Paddlewheel Units. *Inorg. Chem.* **2010**, *49*, 695–703. [[CrossRef](#)] [[PubMed](#)]
29. Julve, M.; Gleizes, A.; Chamoreau, L.M.; Ruiz, E.; Verdager, M. Antiferromagnetic Interactions in Copper(II) μ -Oxalato Dinuclear Complexes: The Role of the Counterion. *Eur. J. Inorg. Chem.* **2018**, *2018*, 509–516. [[CrossRef](#)]
30. Demakov, P.A. Properties of Aliphatic Ligand-Based Metal–Organic Frameworks. *Polymers* **2023**, *15*, 2891. [[CrossRef](#)]
31. Svetogorov, R.D.; Dorovatovskii, P.V.; Lazarenko, V.A. Belok/XSA Diffraction Beamline for Studying Crystalline Samples at Kurchatov Synchrotron Radiation Source. *Cryst. Res. Technol.* **2020**, *55*, 1900184. [[CrossRef](#)]
32. Lazarenko, V.A.; Dorovatovskii, P.V.; Zubavichus, Y.V.; Burlov, A.S.; Koshchienko, Y.V.; Vlasenko, V.G.; Khrustalev, V.N. High-Throughput Small-Molecule Crystallography at the ‘Belok’ Beamline of the Kurchatov Synchrotron Radiation Source: Transition Metal Complexes with Azomethine Ligands as a Case Study. *Crystals* **2017**, *7*, 325. [[CrossRef](#)]
33. Kabsch, W. XDS. *Acta Cryst.* **2010**, *D66*, 125–132. [[CrossRef](#)] [[PubMed](#)]
34. Sheldrick, G.M. SHELXT–Integrated space-group and crystal-structure determination. *Acta Cryst.* **2015**, *A71*, 3–8. [[CrossRef](#)] [[PubMed](#)]
35. Sheldrick, G.M. Crystal structure refinement with SHELXL. *Acta Cryst.* **2015**, *C71*, 3–8. [[CrossRef](#)] [[PubMed](#)]
36. Spek, A.L. Single-crystal structure validation with the program PLATON. *J. Appl. Crystallogr.* **2003**, *36*, 7–13. [[CrossRef](#)]

37. Kumagai, H.; Akita-Tanaka, M.; Inoue, K.; Takahashi, K.; Kobayashi, H.; Vilminot, S.; Kurmoo, M. Metal–Organic Frameworks from Copper Dimers with *cis*- and *trans*-1,4-Cyclohexanedicarboxylate and *cis,cis*-1,3,5-Cyclohexanetricarboxylate. *Inorg. Chem.* **2007**, *46*, 5949–5956. [[CrossRef](#)] [[PubMed](#)]
38. Demakov, P.A.; Bogomyakov, A.S.; Urlukov, A.S.; Andreeva, A.Y.; Samsonenko, D.G.; Dybtsev, D.N.; Fedin, V.P. Transition Metal Coordination Polymers with *Trans*-1,4-Cyclohexanedicarboxylate: Acidity-Controlled Synthesis, Structures and Properties. *Materials* **2020**, *13*, 486. [[CrossRef](#)] [[PubMed](#)]
39. Bleaney, B.; Bowers, K.D. Anomalous paramagnetism of copper acetate. *Proc. R. Soc. Lond.* **1952**, *A214*, 451–465. [[CrossRef](#)]
40. Shen, L.; Yang, S.W.; Xiang, S.; Liu, T.; Zhao, B.; Ng, M.F.; Göettlicher, J.; Yi, J.; Li, S.; Wang, L.; et al. Origin of Long-Range Ferromagnetic Ordering in Metal–Organic Frameworks with Antiferromagnetic Dimeric-Cu(II) Building Units. *J. Am. Chem. Soc.* **2012**, *134*, 17286–17290. [[CrossRef](#)]
41. Hatfield, W.E. New magnetic and structural results for uniformly spaced, alternately spaced, and ladder-like copper (II) linear chain compounds. *J. Appl. Phys.* **1981**, *52*, 1985–1990. [[CrossRef](#)]
42. Calvo, R.; Rapp, R.E.; Chagas, E.; Sartoris, R.P.; Baggio, R.; Garland, M.T.; Perec, M. 1-D Polymers with Alternate Cu₂ and Ln₂ Units (Ln = Gd, Er, Y) and Carboxylate Linkages. *Inorg. Chem.* **2008**, *47*, 10389–10397. [[CrossRef](#)] [[PubMed](#)]
43. Baggio, R.; Calvo, R.; Garland, M.T.; Peña, O.; Perec, M.; Slep, L.D. A new copper (II) di- μ_2 -carboxylato bridged dinuclear complex: [Cu(oda)phen]₂·6H₂O (oda = oxydiacetate, phen = phenanthroline). *Inorg. Chem. Commun.* **2007**, *10*, 1249–1252. [[CrossRef](#)]
44. Agterberg, F.P.; Provó Kluit, H.A.; Driessen, W.L.; Oevering, H.; Buijs, W.; Lakin, M.T.; Spek, A.L.; Reedijk, J. Dinuclear Paddle-Wheel Copper(II) Carboxylates in the Catalytic Oxidation of Carboxylic Acids. Unusual Polymeric Chains Found in the Single-Crystal X-ray Structures of [Tetrakis(μ -1-phenylcyclopropane-1-carboxylato-O,O')bis(ethanol-O)dicopper(II)] and catena-Poly[[bis(μ -diphenylacetato-O,O')dicopper](μ_3 -diphenylacetato-1-O:2-O':1'-O')(μ_3 -diphenylacetato-1-O:2-O':2'-O')]. *Inorg. Chem.* **1997**, *36*, 4321–4328. [[CrossRef](#)] [[PubMed](#)]

Disclaimer/Publisher’s Note: The statements, opinions and data contained in all publications are solely those of the individual author(s) and contributor(s) and not of MDPI and/or the editor(s). MDPI and/or the editor(s) disclaim responsibility for any injury to people or property resulting from any ideas, methods, instructions or products referred to in the content.